www.sciencemag.org/content/358/6368/1299/suppl/DC1

Supplementary Material for

A precise measurement of the magnetic field in the corona of the black hole binary V404 Cygni

Yigit Dallilar,* Stephen S. Eikenberry,* Alan Garner, Richard D. Stelter, Amy Gottlieb, Poshak Gandhi, Piergiorgio Casella, Vik S. Dhillon, Tom R. Marsh, Stuart P. Littlefair, Liam Hardy, Rob Fender, Kunal Mooley, Dominic J. Walton, Felix Fuerst, Matteo Bachetti, A. J. Castro-Tirado, Miguel Charcos, Michelle L. Edwards, Nestor M. Lasso-Cabrera, Antonio Marin-Franch, S. Nicholas Raines, Kendall Ackley, John G. Bennett, A. Javier Cenarro, Brian Chinn, H. Veronica Donoso, Raymond Frommeyer, Kevin Hanna, Michael D. Herlevich, Jeff Julian, Paola Miller, Scott Mullin, Charles H. Murphey, Chris Packham, Frank Varosi, Claudia Vega, Craig Warner, A. N. Ramaprakash, Mahesh Burse, Sujit Punnadi, Pravin Chordia, Andreas Gerarts, Héctor de Paz Martín, María Martín Calero, Riccardo Scarpa, Sergio Fernandez Acosta, William Miguel Hernández Sánchez, Benjamin Siegel, Francisco Francisco Pérez, Himar D. Viera Martín, José A. Rodríguez Losada, Agustín Nuñez, Álvaro Tejero, Carlos E. Martín González, César Cabrera Rodríguez, Jordi Molgó, J. Esteban Rodriguez, J. Israel Fernández Cáceres, Luis A. Rodríguez García, Manuel Huertas Lopez, Raul Dominguez, Tim Gaggstatter, Antonio Cabrera Lavers, Stefan Geier, Peter Pessev, Ata Sarajedini

*Corresponding author. Email: ydallilar@ufl.edu (Y.D.); eiken@ufl.edu (S.S.E.)

Published 8 December 2017, *Science* **358**, 1299 (2017)
DOI: 10.1126/science.aan0249

This PDF file includes:

Other Supplementary Material for this manuscript includes the following:
(available at www.sciencemag.org/content/358/6368/1299/suppl/DC1)

Data File S1 as a separate .zip file

Materials and Methods

Near-Infrared Observations

We obtained near-infrared observations with the Canarias Infrared Camera Experiment (CIRCE) on the 10.4-meter Gran Telescopio Canarias (*15*), the full lightcurve is represented in Fig. 1. We performed observations in fast photometry mode with 10 Hz time-resolution in the *Ks* filter. The detector was configured to take 120 sequential reads on a band of 128 pixels (~13 arcsec) wide, which were cleared with a fast reset between every six reads. We deliberately defocused the telescope to reduce non-linearity effects due to the target brightness (<8 mag in the *Ks* band). The telescope pointing was dithered between each readout sequence to allow subtraction of the variable infrared sky background. The apparent gaps in the lightcurve shown in Fig. 1 are due to this procedure.

We applied standard full-frame near-infrared data reduction procedures to reduce the images: dark subtraction, linearity correction, flat fielding, sky subtraction, bad pixel removal and cosmic-ray event detection/removal. Pick-up noise was removed from the images by modeling master even/odd channel noise patterns. Final images were provided by an image subtraction procedure to obtain the source count rate for each 0.1 second time interval. We used an aperture measuring 35 pixels in diameter to perform aperture photometry on both V404 Cygni and a reference star (2MASS J20240376+3351562, ra=20:24:03.769 dec=33:51:56.27), which has *Ks*=11.8 mag (*21*) and is used for flux calibration.

Optical Observations

We carried out optical observations with the high-speed optical imager ULTRACAM (*16*) at the 4.2-m William Herschel Telescope simultaneously in three bands (*u', g', r'*). The instrument was configured in its drift mode to provide fast imaging with 35.9 ms time resolution (with exposure time of 34.8 ms and dead time of 1.1 ms) on a window size of ~50×50 pixels**.** In the *u'* band only, we picked the frame time as 15x35.9 ms to improve signal to noise ratio. A comparison star, URAT1 620-473466 (ra=20:23:56.44, dec=33:48:16.9) (*30*), was included in the field of view to correct for transparency variations and remove the effects of long-term airmass variations during the course of observation, although airmass was restricted to ≤1.1.

The observations were reduced with ULTRACAM pipeline v.9.4 software (*16*), including bias subtraction and flat fielding. For photometric extraction, fixed aperture sizes were preferred and the centroid position of V404 Cygni was tracked for each frame. The clipped-mean value in an annulus centered on the target is used to determine the sky level (see ref. (*12*) for details).

Radio Observations

The Arcminute Microkelvin Imager Large Array (AMI-LA) (*19*) observed V404 Cygni extensively throughout its 2015 outburst at frequencies between 12-18 GHz. The

observing campaign was carried out as part of the University of Oxford's 4 PI SKY (*31*) transients programme. J2023+3153 (ra= 20:23:19.02 dec=31:53:02.30) and 3C48 were used as complex gain and flux/bandpass calibrators respectively during the observations. Flagging and calibration of the data were performed with the AMI REDUCE software(*32, 33*). The calibrated data were then imported into CASA(*34*) and the flux densities of V404 Cygni were extracted by vector averaging over all baselines at multiple frequencies within the passband.

We extracted the V404 Cygni light curve at 13.9 GHz, 15.4 GHz and 16.9 GHz between MJD 57198.18 and 57198.25 at intervals of 80 seconds. The light curve shows a gradual rise in flux density, from 200 mJy to 1.8 Jy over a span of ~80 minutes, as shown in Fig. 1. The spectrum between 13.9 GHz and 16.9 GHz changes from near-flat to a relatively steep optically thick spectrum.

X-ray Spectra

The X-ray data were obtained with the NuSTAR observatory (*17*), which covers the 3-79 keV bandpass, and are reduced following the procedure described in ref. (*18*). In brief, the unfiltered event files were cleaned using NUPIPELINE, part of the NUSTARDAS(*17*) software package (using software version 1.5.1 and caldb version 20150316). We then extracted the spectrum from the small X-ray flare seen just before minute 68 in Fig. 2 from a circular region of radius 160" with NUPRODUCTS which also computes the appropriate instrumental response files. This is shown in Fig. 4.

Sub-second X-ray Lightcurve

Typically, the full information needed to calculate the live observation time (excluding dead time) of a NuSTAR observation contains some events vetoed by the anti-coincidence system, plus a small fraction of dead time from housekeeping operations. This precise information is not telemetered to the ground, and only the total livetime of each second of observation is available to the observer. For this reason, the tool NULIVETIME is only able to obtain livetime-corrected light curves with a sampling time of multiples of 1 sec (*35*).

However, if the source is as bright as V404 Cygni during our observation, dead time is predominantly from source events. It is thus possible to use the PRIOR column in the unfiltered event files (with the _uf extension in the observation directory) to get a sufficiently precise estimate of the live time from event to event, and obtain an estimate of total live time with a bin time of less than 1 sec (*36*). We executed this procedure with the MaLTPyNT software and obtained X-ray lightcurve for energy ranges 3-10 keV and 10-79 keV with ~35.9 ms time resolution (*37*).

Dereddened OIR Lightcurves

We adopt the most recent visual extinction value, A_V = 4 mag (*6*), to V404 Cygni to correct for reddenning by interstellar dust. We used the Milky Way average value of the total-to-selective extinction parameter R_V = 3.1 (*38*) to translate this extinction into the filters used in our observations.

Radio/OIR Spectra

In Fig. 4, we show OIR fluxes in terms of excess emission just before the decay event relative to the post-decay values, because there is no clear evidence of post-decay emission having synchrotron origin. Hence, OIR flux values are reported as the difference between 1 minute of integrated flux ending with the beginning of the decay event (57198.2258-57198.2265 MJD), and the next, starting with the leveling off of OIR flux (57198.2286-57198.2293 MJD). Given that radio flux at the beginning of our observations is much dimmer than the radio emission just before the decay event, the radio emission has a pure synchrotron origin as a result of 30 minutes of jet activity. Therefore, the nearest radio flux measurements to the former time interval are shown in the figure.

Lightcurve Fitting

We model the decay-only portion of the de-reddened OIR lightcurves with an exponential decay with equation $f(t) = A\exp(-(t-B)/\tau_\nu) + C$, in which the cooling timescale (τ_ν) is the only parameter of interest for our study. The measurement errors $(\Delta\tau_\nu)$ are obtained from the model covariance matrix propagated from the flux errors in the lightcurves via a least-square minimization procedure. The larger uncertainties in the *u'* band are due to the degraded time resolution and signal-to-noise ratio compared to other bands, due to lower instrument throughput and source flux. The *Ks* timescale uncertainty is partially due to the time gaps in our observed lightcurve. We perform the fits over the same time interval for all OIR bands. The start time coincides with the beginning of the next IR sequence just after the small OIR flare, in order to use the longest baseline available.

We split the X-ray observation into two energy bands: soft X-rays (3-10 kev) and hard X-rays (10-79 keV). We determine the effective energies by calculating the median energy of the observed counts in each energy band, finding 6.4 and 15.6 keV respectively. In the X-ray, we consider both statistical errors and systematic errors from the uncertainty in the start time of the decay fit. For the statistical errors, we perform 10^6 iterations of a Monte Carlo simulation, in which we create simulated lightcurves by taking the observed curve and adding Gaussian noise to each data point, drawn from a distribution with σ equal to the Poisson error in each time bin. We then measure the standard deviation of the timescale measurements, each determined via least-square fitting with a constant starting time (57198.22712 MJD), over the simulated lightcurves. We estimate the systematic errors by changing the starting point of the fit time interval

(from 57198.22710 to 57198.22713 MJD - a span of ~2.5s), and determining the best-fitting decay time constant. We find random errors of ±0.08/0.13 seconds in soft/hard X-rays, and systematic errors of ±0.7/0.6 seconds.

Continuum Subtraction

The faint OIR flare just before the synchrotron cooling decay is shown in Fig. S2. We smooth the OIR lightcurves (except the *u'* band due to degraded time resolution) by re-binning them into time intervals of 3 seconds. Thus, we are able to detect discrete fast flaring activities shorter than 3 seconds and interpolate over these time intervals using the adjacent continuum level. We then derive a flare-only lightcurve by subtracting the smoothed continuum from the original data. The X-ray lightcurve is excluded from this procedure, primarily due to the close proximity between the possible X-ray emission counterpart and the following decay.

As shown in Fig. S2, we observe a faint OIR flare with amplitude ~0.1 Jy coincident in time in the *g'*, *r'* and *Ks* bands. This flare is undetected in *u'* band due to the lower signal-to-noise at high time resolution. This small flare is slightly delayed (~3-4 s) after, and similar in duration to, the X-ray flare. This is broadly consistent with a thermal reprocessing signature whereby the X-ray flux briefly heats the surface of some portion of the accretion disk and/or companion star. Alternatively, this could also be a time-delayed flare due to injection of energy (e.g. by an internal shock) into a relativistic jet outflow, similar to those seen in GRS1915+105 (*39*).

Synchrotron Cooling

The energy-loss rate of relativistic electrons via synchrotron cooling is given by (*40*),

$$-\frac{d\gamma}{dt} = \frac{\sigma_T B^2 \gamma^2}{6\pi m_e c} = \alpha_\gamma \gamma^2 \qquad \text{Eq. S1}$$

where σ_T is the Thomson scattering cross-section, γ is the Lorentz factor of the electrons, m_e is the mass of a single electron, c is the speed of light and t is time. We approximate the frequency of the emitted radiation using gyration frequency (ν_g) as $\nu \sim \gamma^2 \nu_g$ from ref. (*41*), and derive the synchrotron cooling timescale from the relation $\tau_{sync,\nu} = \nu/(d\nu/dt)$,

$$\tau_{sync,\nu} = \frac{1}{2\alpha_\gamma}\sqrt{\frac{\nu_g}{\nu}} \propto B^{-3/2}\nu^{-1/2} \qquad \text{Eq. S2}$$

With the values of $\alpha_\gamma = 2.5\times10^{-11}(B/1\text{ G})^2\text{ s}^{-1}$ and $\nu_g = 2.8\times10^{6}(B/1\text{ G})$ Hz, we evaluate the expression for the cooling timescale,

$$\boldsymbol{\tau_{sync,\nu} = 3.35\times10^{6}\left(\frac{B}{1\ \mathrm{G}}\right)^{-\frac{3}{2}}\left(\frac{\nu}{10^{14}\ \mathrm{Hz}}\right)^{-\frac{1}{2}}\ \mathrm{seconds}} \qquad \text{Eq. S3}$$

Firstly, we fit the frequency versus timescale data in 6 bands (from OIR to X-ray) to an equation in the form $\tau = A\,\nu^{p}$ where A and p are free parameters. We determine $p = -0.49 \pm 0.03$ with a least-squares fitting algorithm, consistent (within ~1σ) with the value expected for synchrotron cooling.

We then evaluate the corresponding individual magnetic field values for all bands:

$$\boldsymbol{B_{\nu} = 2.24\times10^{4}\left(\frac{\tau}{1\ \mathrm{sec}}\right)^{-\frac{2}{3}}\left(\frac{\nu}{10^{14}\ \mathrm{Hz}}\right)^{-\frac{1}{3}}\ \mathrm{Gauss}} \qquad \text{Eq. S4}$$

By propagating the uncertainty estimates for the timescales in Table S1, we determine the best-fitting magnetic field (B_0) as 461±12 Gauss with $\chi^2_{\upsilon} = 0.8$ per degree of freedom. Over timescales of seconds in the X-ray to minutes in the OIR bands, there is no evidence for a varying magnetic field. Accordingly, we report fractional variation in the form, $\Delta B/B = (B_{X-ray} - B_0)/B_0 < 15\%$.

Thermal vs Non-Thermal Emission

We consider the possibility that the primary OIR emission from V404 Cygni during this event might arise from thermal blackbody processes, including X-ray reprocessing [as has been previously suggested (*11*)]. The OIR emission generally peaks in the *r′* band, with slightly lower flux in the *g′* band. The best-fitting temperature for the *g′–r′* color is T = 5500 K. At higher temperatures, T>5700 K, the *g′* flux would match that in *r′* (contrary to the observed peak in *r′*), so we adopt this as an upper limit on the temperature.

From this upper limit on the color temperature (T_c) of 5500+200 K, we can calculate the emitting surface area required to produce the observed luminosity from V404 Cygni (as the distance is precisely known), and then convert this to a minimum radius $R \leq (A/\pi)^{1/2}$.

In Fig. S1, we compare these blackbody radii to the measured OIR decay timescales. The decay timescales limit the light-crossing radius as $R < 1.25c\tau$ in the limiting case of a face-on circular region due to causality. While the allowed radii for the *Ks*-band are compatible with thermal emission, the other bands are not: they show differences by up to a factor of 2 in the radii even at the upper/lower uncertainty limits. A χ^2 analysis gives a confidence interval of probability < 7×10^{-8}, allowing us to reject the hypothesis that thermal emission can produce the observed fluxes and decay timescales. The observed flux is simply too bright and too red to be explained by thermal emission from such small regions.

Comptonization vs Synchrotron Cooling

The relative efficiency of synchrotron versus Compton processes in cooling relativistic electrons is equal to the ratio of magnetic energy density to photon energy density at the location of the relevant electrons. Using the value for the magnetic field under the synchrotron cooling model in Fig. 3, the energy density stored in the magnetic field is straightforward to calculate as

$$\boldsymbol{u_B = (B_0)^2/8\pi \sim 8.4{\times}10^3\ \ ergs/cm^3} \qquad \text{Eq. S5}$$

The photon density at this location is more difficult to estimate, as it depends on the relative geometry of the system - particularly the distance between the relativistic electrons and the source of the cooling photons. The most conservative assumption (i.e. maximizing the inferred photon energy density at the electron location) would be to assume that the full luminosity seen from V404 Cygni during this event arises in a region concentric with the electron population in question. This would be the case for synchrotron self Compton (SSC) processes, for example. We proceed with this assumption for now, noting that the derived photon energy density will be a firm upper limit on the local u_p, and thus a lower limit on the relative ratio of synchrotron versus Compton processes, u_B/u_p .

Given the relatively flat spectral energy distribution (~ 1 Jy) from radio to OIR, with an apparent spectral break at frequency 5x10^{14} Hz, the photon energy density is dominated by the flux density at/near the break. Thus, the corresponding photon energy density of the radiation is given by,

$$\boldsymbol{u_p = \frac{L_\nu}{4\pi R^2 c} = \frac{\nu F_\nu\, 4\pi d^2}{4\pi R^2 c} = \frac{\nu F_\nu d^2}{cR^2}} \qquad \text{Eq. S6}$$

where we can estimate the size of the region (R) using the light-crossing timescale, $R \sim 1.25\, c\tau$ using the values in Table S1, d is the distance to V404 Cygni of 2.39 kpc(*6*) and L_ν is the OIR luminosity of the source.

If we select bands near the OIR frequency break, we have $\nu F_\nu \sim 1.3x10^{-8}$ergs/s/cm^2 for u' band, and $\nu F_\nu \sim 2.1x10^{-8}$ ergs/s/cm^2 for g' band - confirming that the exact choice of band has a relatively small impact on the actual value of L_ν. Taking the values of τ for these bands from Table S1 and using the relation $R \sim 1.25\, c\tau$, we arrive at values of $u_p \sim 1.6$ ergs/cm^3 and $u_p \sim 0.7$ ergs/cm^3, respectively, for g' and u' bands. These give values of the relative efficiency of synchrotron cooling versus Compton cooling

$$\boldsymbol{\eta = \frac{u_B}{u_p} > 500} \qquad \text{Eq. S7}$$

This confirms that the observations are consistent with the scenario that synchrotron cooling dominates over Compton cooling during this event, with a magnetic field

strength of 461 Gauss. In fact, even if we were to assume that all of the long-wavelength radiation arises from a region as small as the X-ray timescale of τ~1.8s, we still find values of η~3. Thus, even under very conservative assumptions, synchrotron cooling is expected to dominate Compton processes for this event - a conclusion which is also confirmed by the $\nu^{-1/2}$ dependence of the timescales shown in Fig. 3.

Electron Population

The relation between spectral index of the jet emission ($F_\nu \propto \nu^\alpha$) and energy distribution of the electrons ($N(E) = \kappa E^{-p}$) is given by $\alpha = (p-1)/2$, therefore, $p \sim 1$ for a flat spectral distribution of the emitted radiation. Normalization of the *N*(*E*) relation can be obtained from the equation (*41*),

$$\boldsymbol{\kappa \sim 3{\times}10^{40}\left(\frac{F_\nu}{1\ \mathrm{Jy}}\right)\left(\frac{B}{450\ \mathrm{G}}\right)^{-1}} \qquad \text{Eq. S8}$$

We denote the electron properties with the following assumptions;
$E_{\min} \ll E_{\max}$ and $\gamma m_e c^2 = \sqrt{(\nu/\nu_g)} m_e c^2$. Thus, the total energy in the electrons is,

$$\boldsymbol{E_e \sim 3{\times}10^{40}\int_{E_{\min}}^{E_{\max}} E^{-1} E\, dE = 2.2{\times}10^{37}\left(\frac{\nu}{10^{15}\ \mathrm{Hz}}\right)^{1/2}\ \mathrm{ergs}} \qquad \text{Eq. S9}$$

or in terms of densities,

$$\boldsymbol{u_e \sim \frac{E_e}{V} = 2.4{\times}10^{4}\left(\frac{\nu}{10^{15}\ \mathrm{Hz}}\right)^{1/2}\left(\frac{\tau}{2\ \mathrm{sec}}\right)^{-3}\ \mathrm{ergs/cm^3}} \qquad \text{Eq. S10}$$

We show the spectral energy density distribution of the electron population in Fig. S3, using the value of κ from above and $p \sim 1$. The dashed lines are used to visually connect X-ray and radio regimes with the predicted slopes from the values in Fig. 4.

Size of the Radio Photosphere

Synchrotron cooling arguments predict a cooling timescale two orders of magnitude longer in the radio regime (about 6-7 hours) than in the OIR regime. Our radio observations truncate after about two and a half hour from the offset time in Fig. 1, and, in fact, a second major radio burst starts in 2 hours. Therefore, we cannot provide timescale estimates for radio emission. Instead, we rely on self-absorbed radio emission, and we adopt a method (*42*) previously used to estimate sizes for extra-galactic self-absorbed synchrotron radio sources, e.g. blazars. The expression for the angular sizes of these sources is,

$$\boldsymbol{\theta = 0.17 \left(\frac{B}{1\ \mu G}\right)^{1/4} \left(\frac{F_{\nu_p}}{1\ Jy}\right)^{1/2} \left(\frac{\nu_p}{1\ MHz}\right)^{-5/4}\ arcsec} \qquad \text{Eq. S11}$$

where ν_p is the peak frequency of the radiation and F_{ν_p} is the corresponding radio flux at the peak frequency. In terms of sizes, we obtain,

$$\boldsymbol{R = 8.9\times10^{12} \left(\frac{B}{1\ G}\right)^{1/4} \left(\frac{F_{\nu_p}}{1\ Jy}\right)^{1/2} \left(\frac{\nu_p}{10^{10}\ Hz}\right)^{-5/4}\ cm} \qquad \text{Eq. S12}$$

Scaling Relations in Equipartition Model

In the equipartition model, the size of the emitting region is proportional to $\boldsymbol{B_{eq}^{-7/6}}$ assuming constant observables (see equation 1 with $\boldsymbol{R \sim c\tau}$). The electron particle density ($\boldsymbol{n_e}$) is proportional to $\boldsymbol{u_e/\gamma_{eff}}$ and, in an equipartition configuration, we can use the relation $\boldsymbol{u_e \sim u_B \propto B_{eq}^2}$. Including $\boldsymbol{\gamma_{eff} \propto \sqrt{\nu/\nu_g} \propto B_{eq}^{-1/2}}$ from the synchrotron cooling section, we find $\boldsymbol{n_e \propto B_{eq}^{5/2}}$. As a result, a lower magnetic field (compared to previous estimates) during this cooling event implies a larger size for the emitting region and substantially lower electron particle density.

Supplementary Figures

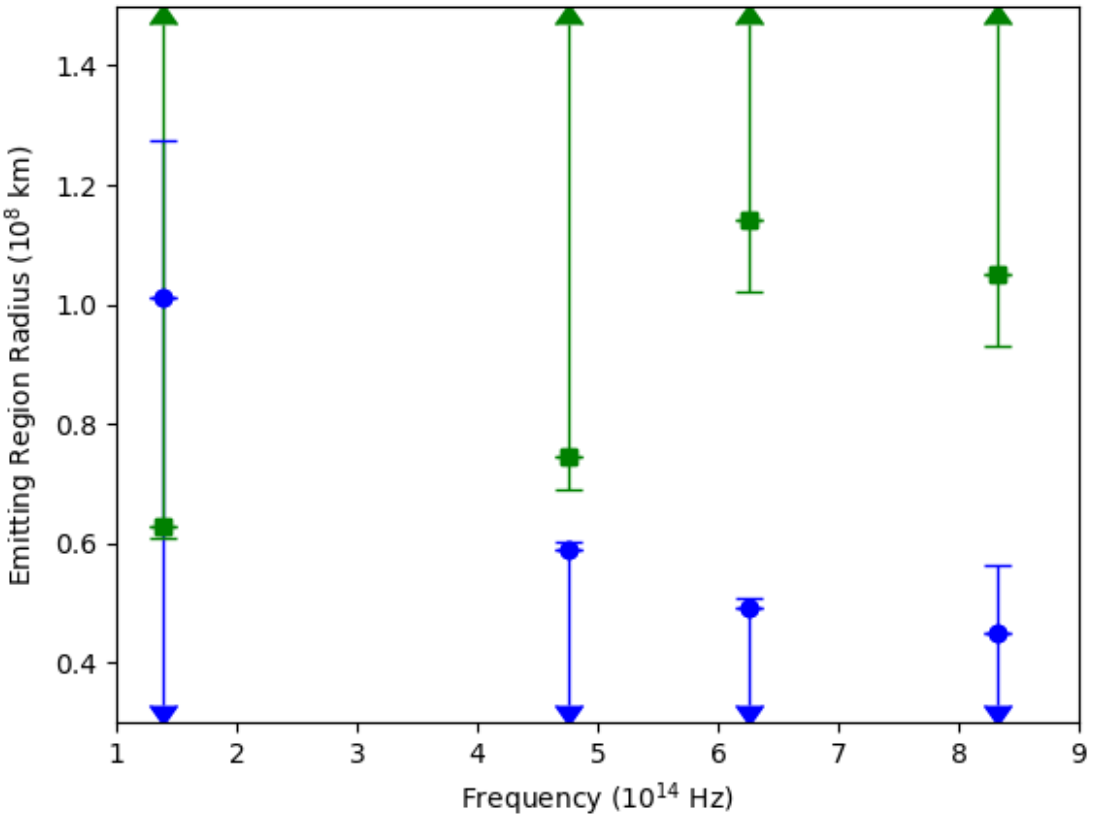

Fig. S1.

Comparison of size estimates from timescale and blackbody arguments. Blue circles indicate the values derived from the lightcurves in Fig. 2 and Table S1 based on causality arguments. Green squares indicate the lower limits required for a blackbody emitter, based on the observed fluxes in each band and the color temperature of T = 5500K with an upper limit of T<5700K (points are at T=5500K, error bars extend to T≤5700K).

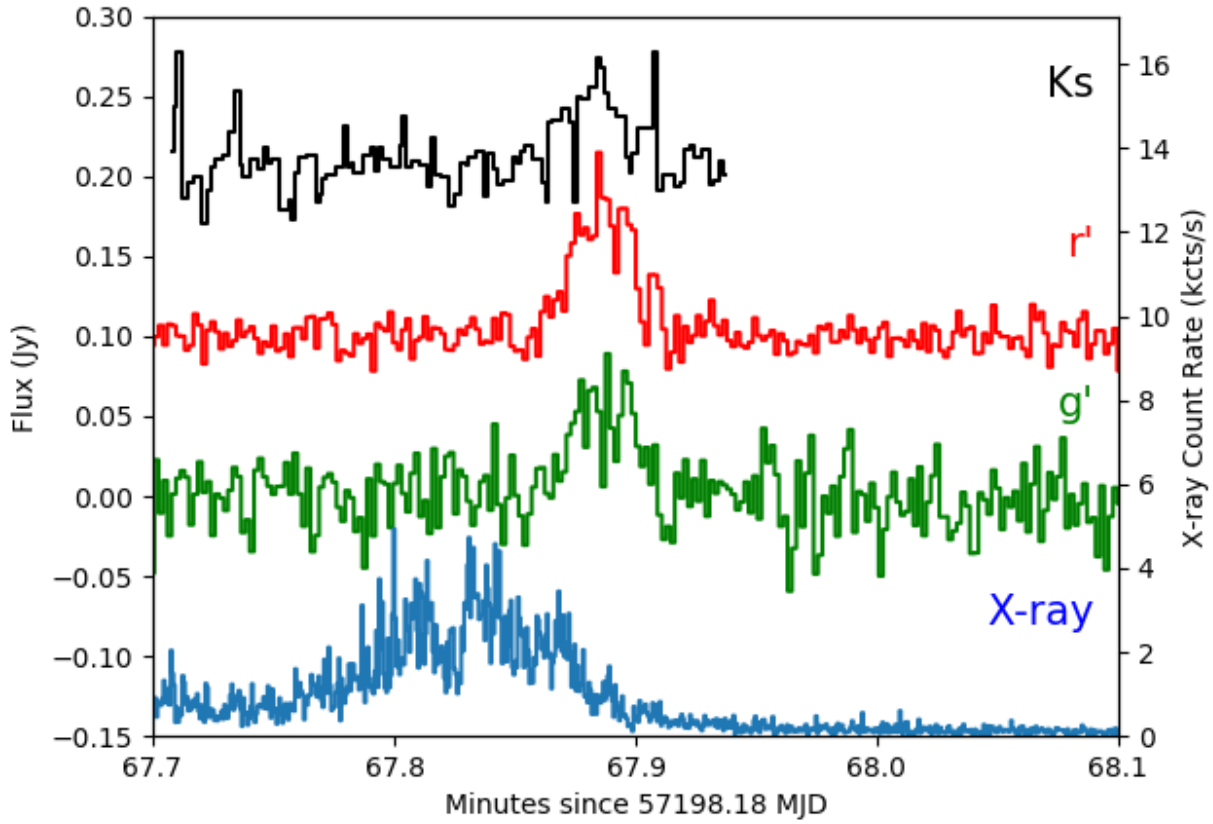

Fig. S2.

Continuum subtracted OIR lightcurves and X-ray (3-10 keV) count rate (in kilocounts per secound) around the OIR flare just before the decay event. Left axis denotes extinction corrected OIR flux (vertically shifted by 0.1 Jy for *r'*, 0.2 Jy for *Ks* filters), whilst the right axis indicates the X-ray count rate.

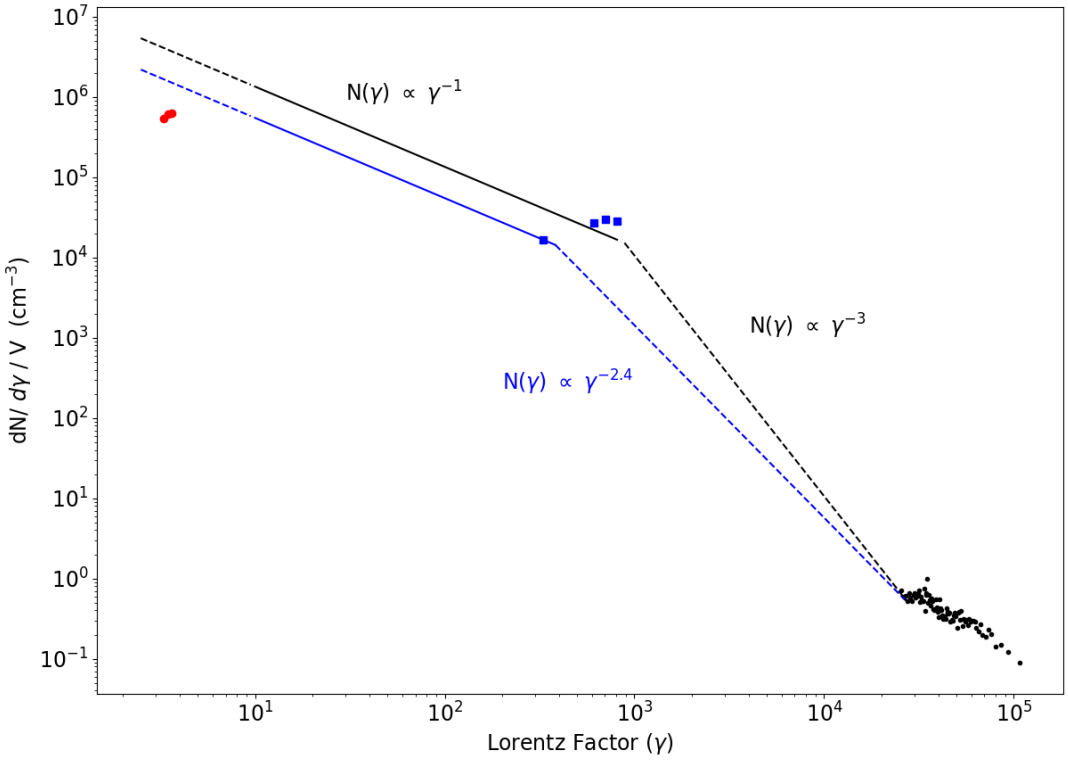

Fig. S3.

The electron density versus Lorentz factor for relativistic electrons present before the decay event. The radio emission region arises from a larger photosphere, and thus the inferred Lorentz factors for the radio-emitting electrons may differ substantially from the red circles shown here.

Table S1. Exponential decay timescales and magnetic field measurements.

Filter	Central Frequency (Hz)	Decay Timescale (s)	Inferred Magnetic Field (G)
Ks	1.39×10^{14}	272 ± 70	479 ± 82
r'	4.76×10^{14}	157 ± 4	458 ± 7
g'	6.25×10^{14}	131 ± 5	472 ± 12
u'	8.33×10^{14}	121 ± 33	452 ± 81
X-ray (3-10 keV)	1.55×10^{18}	1.8 ± 0.7	607 ± 157
X-ray (10-79 keV)	5.03×10^{18}	2.2 ± 0.6	364 ± 68

References and Notes

1. D. L. Meier, The association of jet production with geometrically thick accretion flows and black hole rotation. *Astrophys. J.* **548**, L9–L12 (2001). doi:10.1086/318921

2. S. Markoff, H. Falcke, R. Fender, A jet model for the broadband spectrum of XTE J1118+480. Synchrotron emission from radio to x-rays in the low/hard spectral state. *Astron. Astrophys.* **372**, L25–L28 (2001). doi:10.1051/0004-6361:20010420

3. S. Markoff, M. Nowak, S. Corbel, R. Fender, H. Falcke, Exploring the role of jets in the radio/x-ray correlations of GX 339-4. *Astron. Astrophys.* **397**, 645–658 (2003). doi:10.1051/0004-6361:20021497

4. F. Makino, GS 2023+338. *Int. Astron. Union Circ*. no. 4782, B. G. Marsden, Ed. (1989).

5. J. Casares, P. A. Charles, D. H. P. Jones, R. G. M. Rutten, P. J. Callanan, Optical studies of V404 Cyg, the x-ray transient GS2023+338. I. The 1989 outburst and decline. *Mon. Not. R. Astron. Soc.* **250**, 712–725 (1991). doi:10.1093/mnras/250.4.712

6. J. C. A. Miller-Jones, P. G. Jonker, V. Dhawan, W. Brisken, M. P. Rupen, G. Nelemans, E. Gallo, The first accurate parallax distance to a black hole. *Astrophys. J.* **706**, L230–L234 (2009). doi:10.1088/0004-637X/706/2/L230

7. S. D. Barthelmy, A. D'ai, P. D'avanzo, Swift trigger 643949 is V404 Cyg. *The Gamma-ray Coordinates Network Circ*. no. 17929 (2015).

8. H. Negoro *et al.*, MAXI/GSC detection of a new outburst from the Galactic black hole candidate GS 2023+338 (V* V404 Cyg). *The Astronomer's Telegram.* no. 7646 (2015).

9. J. Rodriguez, M. Cadolle Bel, J. Alfonso-Garzón, T. Siegert, X.-L. Zhang, V. Grinberg, V. Savchenko, J. A. Tomsick, J. Chenevez, M. Clavel, S. Corbel, R. Diehl, A. Domingo, C. Gouiffès, J. Greiner, M. G. H. Krause, P. Laurent, A. Loh, S. Markoff, J. M. Mas-Hesse, J. C. A. Miller-Jones, D. M. Russell, J. Wilms, Correlated optical, x-ray, and γ-ray flaring activity seen with INTEGRAL during the 2015 outburst of V404 Cygni. *Astron. Astrophys.* **581**, L9 (2015). doi:10.1051/0004-6361/201527043

10. T. M. Belloni, "States and transitions in black hole binaries" in *The Jet Paradigm: From Microquasars to Quasars* (Springer-Verlag, 2010).

11. M. Kimura, K. Isogai, T. Kato, Y. Ueda, S. Nakahira, M. Shidatsu, T. Enoto, T. Hori, D. Nogami, C. Littlefield, R. Ishioka, Y.-T. Chen, S.-K. King, C.-Y. Wen, S.-Y. Wang, M. J. Lehner, M. E. Schwamb, J.-H. Wang, Z.-W. Zhang, C. Alcock, T. Axelrod, F. B. Bianco, Y.-I. Byun, W.-P. Chen, K. H. Cook, D.-W. Kim, T. Lee, S. L. Marshall, E. P. Pavlenko, O. I. Antonyuk, K. A. Antonyuk, N. V. Pit, A. A. Sosnovskij, J. V. Babina, A. V. Baklanov, A. S. Pozanenko, E. D. Mazaeva, S. E. Schmalz, I. V. Reva, S. P. Belan, R. Y. Inasaridze, N. Tungalag, A. A. Volnova, I. E. Molotov, E. de Miguel, K. Kasai, W. L. Stein, P. A. Dubovsky, S. Kiyota, I. Miller, M. Richmond, W. Goff, M. V. Andreev, H. Takahashi, N. Kojiguchi, Y. Sugiura, N. Takeda, E. Yamada, K. Matsumoto, N. James, R. D. Pickard, T. Tordai, Y. Maeda, J. Ruiz, A. Miyashita, L. M. Cook, A. Imada, M. Uemura, Repetitive patterns in rapid optical variations in the nearby black-hole binary V404 Cygni. *Nature* **529**, 54–58 (2016). doi:10.1038/nature16452 Medline

12. P. Gandhi, S. P. Littlefair, L. K. Hardy, V. S. Dhillon, T. R. Marsh, A. W. Shaw, D. Altamirano, M. D. Caballero-Garcia, J. Casares, P. Casella, A. J. Castro-Tirado, P. A. Charles, Y. Dallilar, S. Eikenberry, R. P. Fender, R. I. Hynes, C. Knigge, E. Kuulkers, K. Mooley, T. Muñoz-Darias, M. Pahari, F. Rahoui, D. M. Russell, J. V. Hernández Santisteban, T. Shahbaz, D. M. Terndrup, J. Tomsick, D. J. Walton, Furiously fast and red: Sub-second optical flaring in V404 Cyg during the 2015 outburst peak. *Mon. Not. R. Astron. Soc.* **459**, 554–572 (2016). doi:10.1093/mnras/stw571

13. T. Shahbaz, D. M. Russell, S. Covino, K. Mooley, R. P. Fender, C. Rumsey, Evidence for magnetic field compression in shocks within the jet of V404 Cyg. *Mon. Not. R. Astron. Soc.* **463**, 1822–1830 (2016). doi:10.1093/mnras/stw2171

14. R. M. Plotkin, J. C. A. Miller-Jones, E. Gallo, P. G. Jonker, J. Homan, J. A. Tomsick, P. Kaaret, D. M. Russell, S. Heinz, E. J. Hodges-Kluck, S. Markoff, G. R. Sivakoff, D. Altamirano, J. Neilsen, The 2015 decay of the black hole x-ray binary V404 Cygni: Robust disk-jet coupling and a sharp transition into quiescence. *Astrophys. J.* **834**, 104 (2017). doi:10.3847/1538-4357/834/2/104

15. S. S. Eikenberry *et al*., arXiv:1709.05542 [astro-ph.IM] (2017).

16. V. S. Dhillon, T. R. Marsh, M. J. Stevenson, D. C. Atkinson, P. Kerry, P. T. Peacocke, A. J. A. Vick, S. M. Beard, D. J. Ives, D. W. Lunney, S. A. McLay, C. J. Tierney, J. Kelly, S. P. Littlefair, R. Nicholson, R. Pashley, E. T. Harlaftis, K. O'Brien, ULTRACAM: An ultrafast, triple-beam CCD camera for high-speed astrophysics. *Mon. Not. R. Astron. Soc.* **378**, 825–840 (2007). doi:10.1111/j.1365-2966.2007.11881.x

17. F. A. Harrison, W. W. Craig, F. E. Christensen, C. J. Hailey, W. W. Zhang, S. E. Boggs, D. Stern, W. R. Cook, K. Forster, P. Giommi, B. W. Grefenstette, Y. Kim, T. Kitaguchi, J. E. Koglin, K. K. Madsen, P. H. Mao, H. Miyasaka, K. Mori, M. Perri, M. J. Pivovaroff, S. Puccetti, V. R. Rana, N. J. Westergaard, J. Willis, A. Zoglauer, H. An, M. Bachetti, N. M. Barrière, E. C. Bellm, V. Bhalerao, N. F. Brejnholt, F. Fuerst, C. C. Liebe, C. B. Markwardt, M. Nynka, J. K. Vogel, D. J. Walton, D. R. Wik, D. M. Alexander, L. R. Cominsky, A. E. Hornschemeier, A. Hornstrup, V. M. Kaspi, G. M. Madejski, G. Matt, S. Molendi, D. M. Smith, J. A. Tomsick, M. Ajello, D. R. Ballantyne, M. Baloković, D. Barret, F. E. Bauer, R. D. Blandford, W. N. Brandt, L. W. Brenneman, J. Chiang, D. Chakrabarty, J. Chenevez, A. Comastri, F. Dufour, M. Elvis, A. C. Fabian, D. Farrah, C. L. Fryer, E. V. Gotthelf, J. E. Grindlay, D. J. Helfand, R. Krivonos, D. L. Meier, J. M. Miller, L. Natalucci, P. Ogle, E. O. Ofek, A. Ptak, S. P. Reynolds, J. R. Rigby, G. Tagliaferri, S. E. Thorsett, E. Treister, C. M. Urry, The *Nuclear Spectroscopic Telescope Array* (*NuSTAR*) high-energy x-ray mission. *Astrophys. J.* **770**, 103 (2013). doi:10.1088/0004-637X/770/2/103

18. D. Walton, K. Mooley, A. L. King, J. A. Tomsick, J. M. Miller, T. Dauser, J. A. García, M. Bachetti, M. Brightman, A. C. Fabian, K. Forster, F. Fürst, P. Gandhi, B. W. Grefenstette, F. A. Harrison, K. K. Madsen, D. L. Meier, M. J. Middleton, L. Natalucci, F. Rahoui, V. Rana, D. Stern, Living on a flare: Relativistic reflection in V404 Cyg observed by NuSTAR during its summer 2015 outburst. *Astrophys. J.* **839**, 110 (2017). doi:10.3847/1538-4357/aa67e8

19. J. T. L. Zwart, R. W. Barker, P. Biddulph, D. Bly, R. C. Boysen, A. R. Brown, C. Clementson, M. Crofts, T. L. Culverhouse, J. Czeres, R. J. Dace, M. L. Davies, R. D'Alessandro, P. Doherty, K. Duggan, J. A. Ely, M. Felvus, F. Feroz, W. Flynn, T. M. O. Franzen, J. Geisbüsch, R. Génova-Santos, K. J. B. Grainge, W. F. Grainger, D. Hammett, R. E. Hills, M. P. Hobson, C. M. Holler, N. Hurley-Walker, R. Jilley, M. E. Jones, T. Kaneko, R. Kneissl, K. Lancaster, A. N. Lasenby, P. J. Marshall, F. Newton, O. Norris, I. Northrop, D. M. Odell, G. Petencin, J. C. Pober, G. G. Pooley, M. W. Pospieszalski, V. Quy, C. Rodríguez-Gonzálvez, R. D. E. Saunders, A. M. M. Scaife, J. Schofield, P. F. Scott, C. Shaw, T. W. Shimwell, H. Smith, A. C. Taylor, D. J. Titterington, M. Velić, E. M. Waldram, S. West, B. A. Wood, G. Yassin, The arcminute microkelvin imager. *Mon. Not. R. Astron. Soc.* **391**, 1545–1558 (2008). doi:10.1111/j.1365-2966.2008.13953.x

20. Materials and methods are available as supplementary materials.

21. R. M. Cutri *et al.*, 2MASS all-sky catalog of point sources. *VizieR Online Data Catalog.* no. 2246 (2003).

22. P. Gandhi, A. W. Blain, D. M. Russell, P. Casella, J. Malzac, S. Corbel, P. D'Avanzo, F. W. Lewis, S. Markoff, M. Cadolle Bel, P. Goldoni, S. Wachter, D. Khangulyan, A. Mainzer, A variable mid-infrared synchrotron break associated with the compact jet in GX 339-4. *Astrophys. J.* **740**, L13 (2011). doi:10.1088/2041-8205/740/1/L13

23. H. C. Spruit, F. Daigne, G. Drenkhahn, Large scale magnetic fields and their dissipation in GRB fireballs. *Astron. Astrophys.* **369**, 694–705 (2001). doi:10.1051/0004-6361:20010131

24. R. Fender, "'Disc-Jet' coupling in black hole X-ray binaries and active galactic nuclei," in *The Jet Paradigm: From Microquasars to Quasars* (Springer-Verlag, 2010).

25. A. A. Zdziarski, The minimum jet power and equipartition. *Mon. Not. R. Astron. Soc.* **445**, 1321–1330 (2014). doi:10.1093/mnras/stu1835

26. L. Stawarz, Y. T. Tanaka, G. Madejski, S. P. O'Sullivan, C. C. Cheung, I. J. Feain, Y. Fukazawa, P. Gandhi, M. J. Hardcastle, J. Kataoka, M. Ostrowski, B. Reville, A. Siemiginowska, A. Simionescu, T. Takahashi, Y. Takei, Y. Takeuchi, N. Werner, Giant lobes of Centaurus A radio galaxy observed with the Suzaku x-ray satellite. *Astrophys. J.* **766**, 48 (2013). doi:10.1088/0004-637X/766/1/48

27. M. Del Santo, J. Malzac, R. Belmont, L. Bouchet, G. De Cesare, The magnetic field in the X-ray corona of Cygnus X-1. *Mon. Not. R. Astron. Soc.* **430**, 209–220 (2013). doi:10.1093/mnras/sts574

28. S. Chaty, G. Dubus, A. Raichoor, Near-infrared jet emission in the microquasar XTE J1550-564. *Astron. Astrophys.* **529**, A3 (2011). doi:10.1051/0004-6361/201015589

29. D. M. Russell, S. Markoff, P. Casella, A. G. Cantrell, R. Chatterjee, R. P. Fender, E. Gallo, P. Gandhi, J. Homan, D. Maitra, J. C. A. Miller-Jones, K. O'Brien, T. Shahbaz, Jet spectral breaks in black hole x-ray binaries. *Mon. Not. R. Astron. Soc.* **429**, 815–832 (2013). doi:10.1093/mnras/sts377

30. N. Zacharias, C. Finch, J. Subasavage, G. Bredthauer, C. Crockett, M. Divittorio, E. Ferguson, F. Harris, H. Harris, A. Henden, C. Kilian, J. Munn, T. Rafferty, A. Rhodes, M. Schultheiss, T. Tilleman, G. Wieder, The first U.S. Naval Observatory Robotic

Astrometric Telescope Catalog. *Astron. J.* **150**, 101 (2015). doi:10.1088/0004-6256/150/4/101

31. 4 PI SKY. Exploring the Transient Universe: https://4pisky.org/

32. M. L. Davies, T. M. O. Franzen, R. D. Davies, R. J. Davis, F. Feroz, R. Génova-Santos, K. J. B. Grainge, D. A. Green, M. P. Hobson, N. Hurley-Walker, A. N. Lasenby, M. López-Caniego, M. Olamaie, C. P. Padilla-Torres, G. G. Pooley, R. Rebolo, C. Rodríguez-Gonzálvez, R. D. E. Saunders, A. M. M. Scaife, P. F. Scott, T. W. Shimwell, D. J. Titterington, E. M. Waldram, R. A. Watson, J. T. L. Zwart, Follow-up observations at 16 and 33-GHz of extragalactic sources from *WMAP* 3-yr data: I—Spectral properties. *Mon. Not. R. Astron. Soc.* **400**, 984–994 (2009). doi:10.1111/j.1365-2966.2009.15518.x

33. Y. C. Perrott, A. M. M. Scaife, D. A. Green, M. L. Davies, T. M. O. Franzen, K. J. B. Grainge, M. P. Hobson, N. Hurley-Walker, A. N. Lasenby, M. Olamaie, G. G. Pooley, C. Rodriguez-Gonzalvez, C. Rumsey, R. D. E. Saunders, M. P. Schammel, P. F. Scott, T. W. Shimwell, D. J. Titterington, E. M. Waldram, AMI Galactic Plane Survey at 16 GHz - I. Observing, mapping and source extraction. *Mon. Not. R. Astron. Soc.* **429**, 3330–3340 (2013). doi:10.1093/mnras/sts589

34. J. P. McMullin, B. Waters, D. Schiebel, W. Young, K. Golap, *Astronomical Data Analysis Software and Systems XVI*, Astronomical Society of the Pacific Conference Series, San Fransisco, California, R. A Shaw, F. Hill, D. J. Bell, Eds. (2007), vol. 376.

35. M. Bachetti, F. A. Harrison, R. Cook, J. Tomsick, C. Schmid, B. W. Grefenstette, D. Barret, S. E. Boggs, F. E. Christensen, W. W. Craig, A. C. Fabian, F. Fürst, P. Gandhi, C. J. Hailey, E. Kara, T. J. Maccarone, J. M. Miller, K. Pottschmidt, D. Stern, P. Uttley, D. J. Walton, J. Wilms, W. W. Zhang, No time for deadtime: Timing analysis of bright black hole binaries with *NuSTAR*. *Astrophys. J.* **800**, 109 (2015). doi:10.1088/0004-637X/800/2/109

36. K. K. Madsen, S. Reynolds, F. Harrison, H. An, S. Boggs, F. E. Christensen, W. W. Craig, C. L. Fryer, B. W. Grefenstette, C. J. Hailey, C. Markwardt, M. Nynka, D. Stern, A. Zoglauer, W. Zhang, Broadband x-ray imaging and spectroscopy of the Crab Nebula and Pulsar with *NuSTAR*. *Astrophys. J.* **801**, 66 (2015). doi:10.1088/0004-637X/801/1/66

37. M. Bachetti, MaLTPyNT: Quick look timing analysis for NuSTAR data. *Astrophysics Source Code Library*. no. 02021B (2015).

38. D. J. Schlegel, D. P. Finkbeiner, M. Davis, Maps of dust infrared emission for use in estimation of reddening and cosmic microwave background radiation foregrounds. *Astrophys. J.* **500**, 525–553 (1998). doi:10.1086/305772

39. S. S. Eikenberry, K. Matthews, E. H. Morgan, R. A. Remillard, R. W. Nelson, Evidence for a disk-jet interaction in the microquasar GRS 1915+105. *Astrophys. J.* **494**, L61–L64 (1998). doi:10.1086/311158

40. Z. L. Uhm, B. Zhang, Fast-cooling synchrotron radiation in a decaying magnetic field and gamma-ray burst emission mechanism. *Nat. Phys.* **10**, 351–356 (2014). doi:10.1038/nphys2932

41. M. S. Longair, *High Energy Astrophysics*. (Cambridge Univ. Press, ed. 3, 2011).

42. A. K. Kambhavi, J. V. Narlikar, *Quasars and Active Galactic Nuclei: An Introduction*. (Cambridge University Press, 1999).